The Frequency Offset Effects of NQR of Spin $I = 1$ for Remote Detection

G. V. Mozjoukhine

Quantum Radiophysics Department, Kaliningrad State University,
ul. Nevskogo, 14, 236040, Kaliningrad

Reprint requests to Dr. G. V. M.; E-mail: mgeorge@gazinter.net

Z. Naturforsch. **57 a,** 297–303 (2002); received January 23, 2002

Presented at the XVIth International Symposium on Nuclear Quadrupole Interactions, Hiroshima, Japan, September 9-14, 2001.

The frequency offset effects of the signal interference during steady-state pulse sequences for remote nuclear quadrupole resonance (NQR) of ^{14}N nuclei were investigated for the purposes of optimization in remote NQR. The experimental investigations with the separation of interfering NQR signals in sequences for observing signals $\{\alpha^{0^\circ}|\beta^{90^\circ} - \tau - \alpha^{180^\circ}|\beta^{90^\circ} - \tau\}$ and $\{\alpha^{0^\circ}|\beta^{90^\circ} - \tau - \alpha^{0^\circ}|\beta^{270^\circ} - \tau\}$ were carried out. The applications of the spherical tensor method for pure NQR of spin $I = 1$ for the investigation of these sequences and one pulse sequence, two pulse sequences are presented, too.

Key words: NQR; Frequency Offset; Multipulse Sequences; FID; Echo; Interference Signal.

Introduction

Nuclear Quadrupole Resonance (NQR) has been investigated for remote detection of explosives and narcotics [1, 2]. The main problem for the detection is the small signal-to-noise ratio (SNR) of the NQR ^{14}N measurements. One method for increasing the SNR is the application of multipulse sequences. Presently the pulse NQR method is used for the remote NQR detection of explosives [3]. It is very difficult to attain the optimal condition for the observation of the temperature of the sample and the optimal parameters of the pulse sequence in case of remote detection. Presently one tries to optimize the multipulse sequence parameters via the computation of the experimental data [4], using the experimental data [3]. The frequency offset effects are important in these data.

Simplest and most widely used is the Carr sequence [5] and its modifications, especially the Strong Off-Resonant Comb (SORC) sequence [6]. These sequences have the following desirable properties: a large number of signals after every pulse and the signal amplitude being approximately one-half of the single pulse decay. The signals of these sequences may be divided into two types: free induction decays (FID) and echoes. When the Carr sequence or SORC sequence is used for the detection of hexahydro-1,3,5-trinitro-s-triazine $C_3H_6N_6O_6$ (RDX), interference of the echo and FID signals takes place. In the notation of Marino, Klainer, and Hirschfeld, these signals are named a-signal and b-signal, respectively [7]. The maximum signal can only be observed if there is a frequency offset: $\Delta f = (n + 1/2)/\tau$, where n is a whole number and τ is the time spacing between the pulses. Therefore the effectivity of the signal accumulation in this sequence depends very much on the offset value. The simple separation of these signals depends upon the relaxation parameters of the NQR sample, i. e. T_2^* (FID time constant), T_2 (spin-spin relaxation time), and T_1 (spin-lattice relaxation time). Moreover, the pulse NQR in the powder has a problem with the 90° and 180° pulses. The durations of 90° and 180° pulses are different for polycrystals. The angles between the radiofrequency field and the axes of the electric field gradient tensor of the polycrystals are accidental [8]. The other problem is the big inhomogeneity of the radiofrequency field in the sample. As a consequence, interference between a- and b-signals takes place in all multipulse sequences for remote detection.

There exist the following ways to avoid the interference of the a- and b-signal. The first way is the computation of the proper signal using different types of multipulse sequences [9]. The second way is the development of a multipulse sequence to remove the

effect of the interference of a- and b-signals [10]. An other method is the application of three-frequency pulse sequences [11, 12].

The detection of landmines does not present a big problem with the application of multipulse sequences in the case of a big volume of the sample, especially for antitank landmines. For example, the quantities of explosives of these landmines are 2.5 kg and 6 kg for the Italian mines TS-2.5 and TS-6. The real problem is the detection of landmines weighing less than 200 g. The inhomogeneity of the radio frequency field is much bigger for such objects. We consider objects which are small compared to the coil.

In this work the results of the spherical tensor method for pure NQR of spin $I = 1$ are exploited for the theoretical investigations. The procedure follows the works of Sanctuary [13]. The applications of this method for the investigation of one pulse- and two pulse-sequences are presented.

Experimental

The experiments were carried out with hexahydro-1,3,5-trinitro-s-triazine $C_3H_6N_6O_6$ (RDX) at room temperature and $NaNO_2$ at 77 K. The experiments were carried out on landmines which contain 150 g of RDX at distances of 5-25 cm. Part of the experiments were carried out with 10 g of RDX inside the solenoidal coil. At room temperature, the experimental NQR frequency of RDX is near 5192 kHz; $T_2^* =$ 1.5 msec, $T_2 = 8$ msec, $T_1 = 10$ msec.

The pulsed NQR-spectrometer has the following specifications: frequency range 0.1 - 30 MHz, pulse length 20 - 250 μs, power of the radio frequency pulses up to 2.5 kW. In this spectrometer we used quadrature detection, quality modulation for damping transient processes in the radio frequency transmitting coil, and damping transient processes in the receiving path. The complete description of this spectrometer is presented in [3]. For the current control of transient processes and the interference level we used the oscilloscope Tektronix TDS 644B (4/1). The radiofrequency coil consists of a flat receive-transmit coil (with an external diameter of 36 cm, and an internal one of 15 cm). The quality of the coil Q is in the range of 360 - 400. To detect NQR signals we used continuous pulse sequences of Steady State Precession [5] (SSFP) with shifting the phase of every second pulse by 180° and without shifting, as well as sequences consisting of composite radio frequency pulses $\{\alpha^{0^\circ}|\beta^{90^\circ} - \tau - \alpha^{180^\circ}|\beta^{90^\circ} - \tau\}$ and $\{\alpha^{0^\circ}|\beta^{90^\circ} - \tau - \alpha^{0^\circ}|\beta^{270^\circ} - \tau\}$, where α, β are the pulse duration; 0°, 90°, 180°, 270° are the initial phase shifts of radiofrequency pulses. The system of forming radiofrequency composite pulses includes a direct digital synthesizer (DDS), created in the S. E. E. corporation Ltd.,Perth, WA, an ordinary personal computer with Intel Pentium Processor 166 MHz, a functional generator (sweep function generator) Hung Chang 9205C, and the software program RUN_DDS EXE, also developed in the S. E. E. corporation Ltd., Perth, WA.

Results and Discussion

We consider the case of the non-axial symmetric pure NQR for $I = 1$ and asymmetry parameter $\eta \neq 0$. This solution is based on the method of Sanctuary [13].

The quadrupole Hamiltonian may be written as [14]

$$H_{\mathrm{Q}} = -\frac{eQq}{4}\sqrt{\frac{(2I+3)(I+1)}{5I(2I-1)}} \cdot \left\{Y^{(2)0}(I) + \eta\left[Y^{(2)2}(I) + Y^{(2)-2}(I)\right]\right\}, \quad (1)$$

where $Y^{(k)q}$ is an irreducible tensor operator, I the spin of nuclei, and eQq the constant of the quadrupole interaction.

The density operator is

$$\sigma = \frac{1}{2I+1}\sum_{k=0}^{2l}\sum_{q=-k}^{k} Y^{(k)q}|I|\Phi_q^k, \quad (2)$$

where Φ_q^k is a time dependent polarization.

The total Hamiltonian is

$$H = H_{\mathrm{Q}} + H_1(t), \quad (3)$$

where

$$H_1(t) = H_{1x}(t) + H_{1y}(t) + H_{1z}(t), \quad (4)$$

$$H_{1x} = \frac{2i}{\sqrt{3}}\omega_{1x}\cos(\omega_x t + \phi_x)(Y^{(1)1} - Y^{(1)-1}),$$

$$H_{1y} = \frac{2i}{\sqrt{3}}\omega_{1y}\cos(\omega_y t + \phi_y)(Y^{(1)1} + Y^{(1)-1}),$$

$$H_{1z} = -i\sqrt{\frac{2}{3}}\omega_{1z}\cos(\omega_z t + \varphi_z)Y^{(1)0}.$$

$$\omega_{1x} = \gamma H_{1x}\sin\theta_x\cos\varphi_x,$$

$$\omega_{1y} = \gamma H_{1y}\sin\theta_y\sin\varphi_y,$$

$$\omega_{1z} = \gamma H_{1z}\cos\theta_z.$$

θ_j, φ_j $(j = x, y, z)$ are the polar angles corresponding to the Z-axis of electric quadrupole gradient tensor. $\omega_{1x}, \omega_{1y}, \omega_{1z}$ are different radio frequency fields with the amplitudes H_{1x}, H_{1y}, H_{1z} and frequencies $\omega_x = \omega_+ + \Delta\omega_+$, $\omega_y = \omega_+ + \Delta\omega_-$, $\omega_z = \omega_0 + \Delta\omega_0$.

$$\omega_0 = \frac{eQq\eta}{2\hbar},\ \omega_+ = \frac{eQq\eta}{4\hbar}(3+\eta),\ \omega_- = \frac{eQq\eta}{4\hbar}(3-\eta)$$

are the transition frequencies in a pure NQR of $I = 1$.

The equation for the density matrix can be expressed as [6]

$$i\hbar\left\langle\left\langle Y^{(k')q'}(I)\left|\sum_{k,q}Y^{(k)q}(I)\partial\Phi_q^{(k)}/\partial t\right\rangle\right\rangle\right. \tag{5}$$

$$\left.= \left\langle\left\langle Y^{(k')q'}(I)\left|\left[H, \sum_{k,q}Y^{(k)q}(I)\Phi_q^{(k)}\right]\right\rangle\right\rangle\right..$$

The complete solutions for one and two pulse sequences are presented in [15].

The FID of a single pulse with frequency ω_+ can be expressed after one pulse as

$$\langle I_x\rangle \sim \frac{\omega_+\omega_{1x}}{\omega_{\text{ef}}}\Big[\sin\omega_{\text{ef}}t_1\sin(\omega_+ t + \varphi_1 - \Delta\omega t_1) \tag{6}$$

$$+\frac{\Delta\omega}{\omega_{\text{ef}}}(1-\cos\omega_{\text{ef}}t_1)\cos(\omega_+ t + \varphi - \Delta\omega t_1)\Big].$$

The NQR signals after the second pulse of a two pulse sequence with a frequency near ω_+ may be written as

$$\text{FID} \sim -\frac{\omega_+\omega_{1x}}{\omega_{\text{ef}}}\Big[1 - \frac{\omega_{1x}^2}{\omega_{ef}^2}(1-\cos\omega_{\text{ef}}t_1)\Big] \tag{7}$$

$$\cdot\Big[\sin\omega_{\text{ef}}t_2\cos(\omega_+(t-\tau-\frac{\Delta\omega}{\omega_+}t_2)+\varphi_2)$$

$$+\frac{\Delta\omega}{\omega_{\text{ef}}}(1-\cos\omega_{\text{ef}}t_2)\sin(\omega_+(t-\tau-\frac{\Delta\omega}{\omega_+}t_2)+\varphi_2)\Big],$$

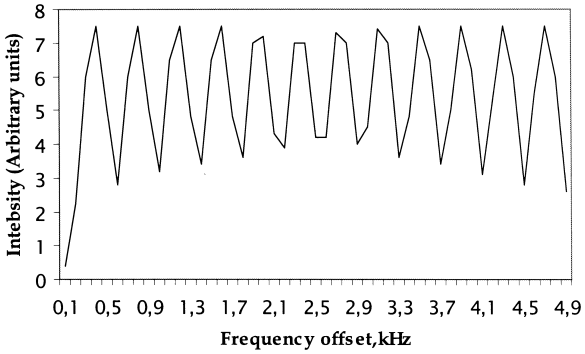

Fig. 1. The model amplitude of the interference signal in a Steady State FID Precession (SSFP) multipulse sequence.

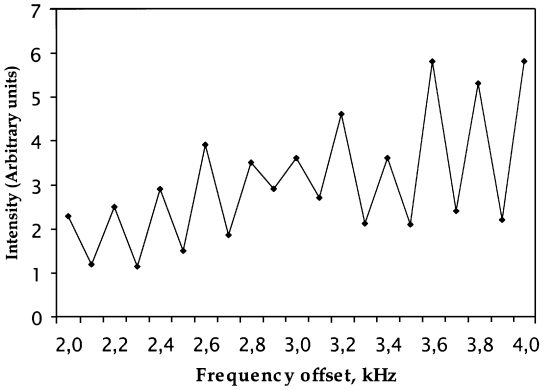

Fig. 2. Experimental plot of the intensities of the SSFP signal with alternate pulses vs. frequency offset. The distance between the model of an antipersonal landmine (150 g of the explosive RDX) and the flat coil is 7 cm.

$$\text{Echo} \sim -\omega_+\frac{\omega_{1x}^3}{\omega_{\text{ef}}^3}(\cos\omega_{\text{ef}}t_2 - 1)\Big\{\frac{\Delta\omega}{\omega_{\text{ef}}}(1-\cos\omega_{\text{ef}}t_1)$$

$$\cdot\cos\Big[\omega_+(t-2\tau-\frac{\Delta\omega}{\omega_+}t_1+\frac{\Delta\omega}{\omega_+}t_2)-\varphi_1+2\varphi_2\Big] \tag{8}$$

$$+\sin\omega_{\text{ef}}t_1\sin\Big[\omega_+(t-2\tau-\frac{\Delta\omega}{\omega_+}t_1+\frac{\Delta\omega}{\omega_+}t_2)$$

$$-\varphi_1+2\varphi_2)\Big]\Big\},$$

where t_1, t_2 are the lengths of the first and the second pulses, τ is the time spacing between the first and the second pulses, φ_1 the phase shift of the first pulse, φ_2 the phase shift of the second pulse, $\Delta\omega$ an offset

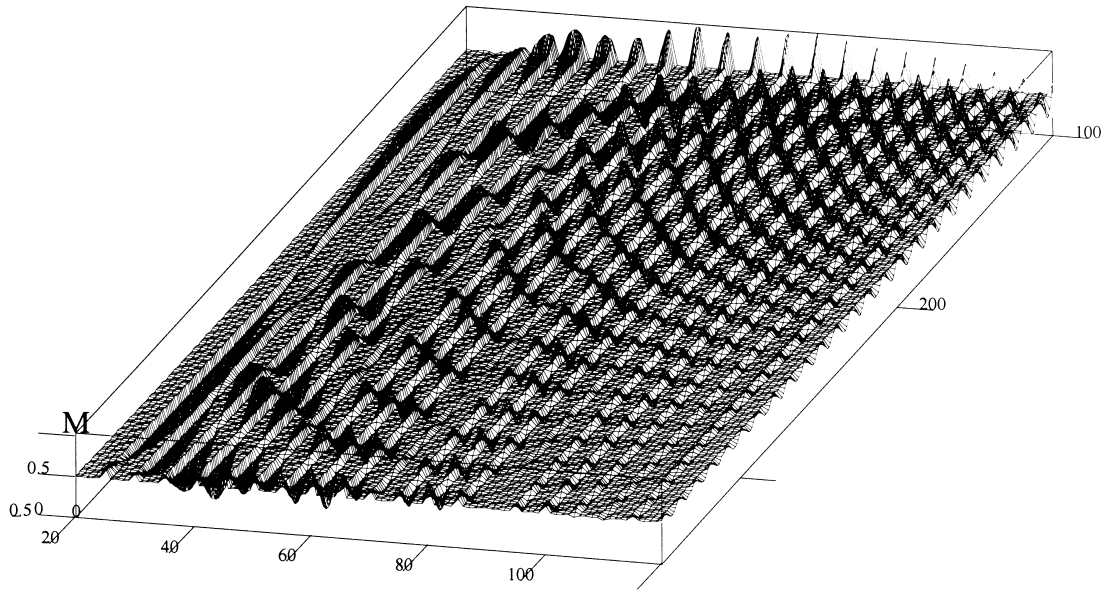

Fig. 3. The surface plot of dependencies. x-axis: time spacing τ is equal 2.50 msec, y-axes: frequency offset Δf has a range up to 10 kHz.

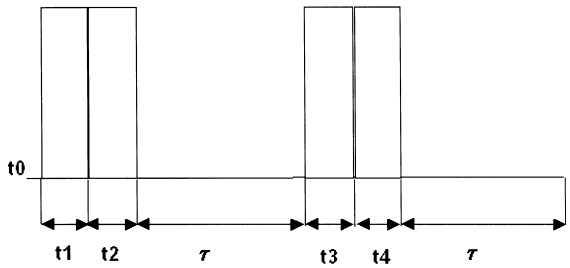

Fig. 4. The composite sequence for the division a- and b-signal.

resonance frequency, $\omega_{\text{ef}} = \sqrt{\Delta\omega^2 + \omega_{1x}^2}$, and $\Delta\omega = \omega_x - \omega_+$.

Usually, the signals of the SORC sequence are presented as [16]

$$V(t) = K_1 e^{t/T_2^*} \cos\Delta\omega t + K_1 e^{(t-\tau)/T_2^*} \cos\Delta\omega(t-\tau). \quad (9)$$

The model amplitude of the interference signal based on (9) is presented in Fig. 1 for the case of τ = 250 msec in RDX. The frequency offset range is 0 - 6 kHz. The experimental measurements of the intensities of the SSFP signal with alternate pulses vs. the frequency offset for remote detection are presented in Figure 2. The distance between the model and an antipersonal landmine is 7 cm. The number of the scans done is 10000. The sample size is 512 g and the sample period 3 μs.

The use of the solutions (6, 7) for modelling a signal produces the 2D plot presented in Figure 3. The comparison of the experimental data with the theoretical formulas (6 - 8) shows that the actual behavior of the superposition signal of the SSFP series is close to the formulas (6, 7).

A method of damping of the negative effect of the superposition signal (9) was proposed in [10]. The sequences consisting of composite radio frequency pulses $\{\alpha^{0^\circ}|\beta^{90^\circ} - \tau - \alpha^{180^\circ}|\beta^{90^\circ} - \tau\}$ and $\{\alpha^{0^\circ}|\beta^{90^\circ} - \tau - \alpha^{0^\circ}|\beta^{270^\circ} - \tau\}$ (Fig. 4) produce the separation of the a- and b-signal in a multipulse sequence. Figure 5 shows this signal in multipulse series. In contrast to numerous research works on composite pulses in NQR [16], the main purpose of composite pulses in this case is to remove the effect of the interference of inductance and echo signals in multipulse sequences of the SORC and SSFP type. During a standard sequence of two spin echo pulses π/2-τ-π it is possible to damp inductance after the second pulse, thus completely removing the interference of inductance and echo signals. When working with the multi-pulse sequence of the SSFP type with equal or nearly equal pulse, there are free induction and echo

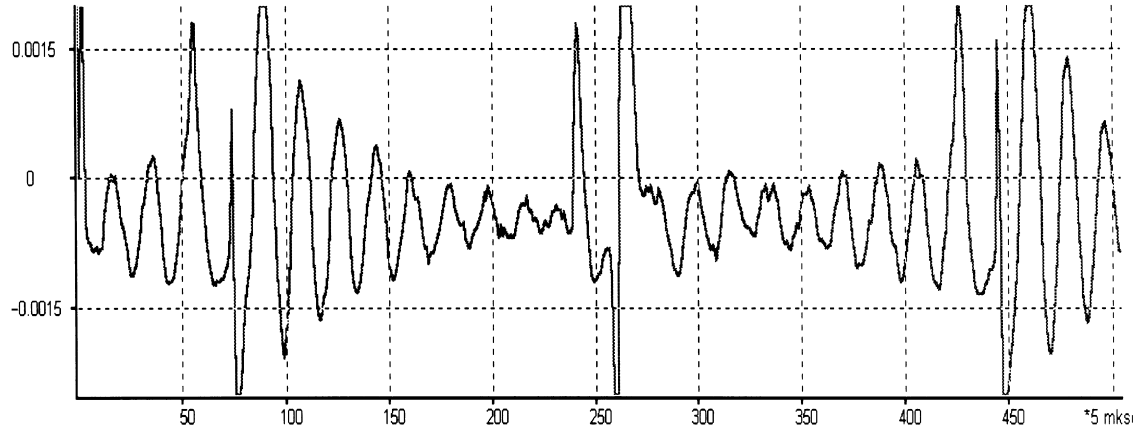

Fig. 5. The oscillogram of the NQR signal in the multipulse sequence $\{\alpha^{0^\circ}|\beta^{90^\circ} - \tau - \alpha^{180^\circ}|\beta^{90^\circ} - \tau\}$, $\alpha = 30$ μs, $\beta = 30$ μs, $n = 1000$, 10 g of RDX, $\tau = 1700$ μs, $\Delta f = 4.9$ kHz.

signals that lead to the interference of echo and FID, as it was said before.

The analysis of these sequences can be carried out by use of the results in (6 - 8). We suppose that the time duration $\alpha = \beta = t_1 = t_2 = t_3 = t_4$ and the radio frequency field define $\omega_{\text{ef}} t_1$ as close to $\pi/2$. In this situation the signal after every composite pulse has three components which can be derived from (6 - 8). The phase shifts $\varphi_1 = 0$ and $\varphi_2 = 90^\circ$ produce the addition of the signals from (6 - 8). The signal from (7) is very small if compared with the other signals. The FID in this case may be written as

$$\text{FID}_{\text{composite}} \propto \frac{\omega_+ \omega_{1x}}{\omega_{\text{ef}}} \left[\left(1 + \frac{\omega_{1x}^2}{\omega_{\text{ef}}^2}\right) \left(\sin \omega_+ t + \frac{\Delta\omega}{\omega_{\text{ef}}} \cos \omega_+ t \right) - \frac{\Delta\omega^2}{\omega_{\text{ef}}^2} \left(\sin \omega_+ t - \frac{\Delta\omega}{\omega_{\text{ef}}} \cos \omega_+ t \right) \right]. \tag{10}$$

We can neglect the term proportional to $\Delta\omega^2/\omega_{\text{ef}}^2$ in this equation. The second composite pulse with the phase shifts $\varphi_3 = 180^\circ$ and $\varphi_4 = 90^\circ$ has only terms proportional to $\Delta\omega^2/\omega_{\text{ef}}^2$. The solutions for echo signals are more complicated. A simple analysis shows that the echoes are caused by the following pairs of pulses: the pulses with pulse length t_1 and t_3, t_1 and t_4, t_2 and t_3, t_2 and t_4. In the case of the pulse sequence $\{\alpha^{0^\circ}|\beta^{90^\circ} - \tau - \alpha^{0^\circ}|\beta^{270^\circ} - \tau\}$, the overlap of these echoes produces an echo which is presented in Figure 5. In the case of pulse sequence

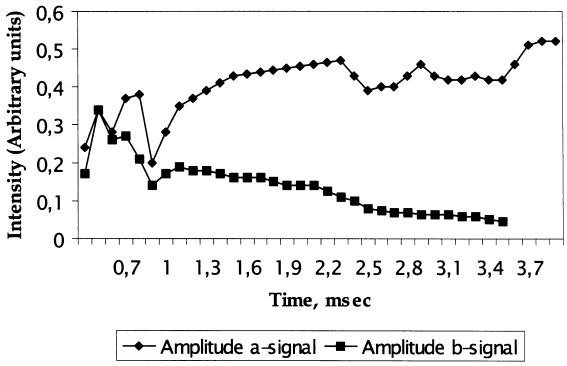

Fig. 6. Amplitude of FID (a-signal) and echo (b-signal) vs. pulse spacing τ for RDX in the $\{\alpha^{0^\circ}|\beta^{90^\circ} - \tau - \alpha^{0^\circ}|\beta^{270^\circ} - \tau\}$ pulse sequence, $t_1 = t_2 = t_3 = t_4 = 35$ μs.

$\{\alpha^{0^\circ}|\beta^{90^\circ} - \tau - \alpha^{180^\circ}|\beta^{90^\circ} - \tau\}$, the echo is probably the result of the action of the first FID and second pair of the pulses.

The amplitude of the FID (a-signal) and the echo (b-signal) vs. the pulse spacing τ for RDX in the $\{\alpha^{0^\circ}|\beta^{90^\circ} - \tau - \alpha^{0^\circ}|\beta^{270^\circ} - \tau\}$ pulse sequence are shown in Figure 6. The main problem in these two sequences consists in the optimization of pulse width. Especially this is important for small time spacing $\tau \leq T_2^*$. Depending on the radio frequency field amplitude, the maximum damping of the interference signal can be achieved when the pulse length and amplitude of radiofrequency field is near the maximum single pulse FID. The sequences $\{\alpha^{0^\circ}|\beta^{90^\circ} - \tau - \alpha^{180^\circ}|\beta^{90^\circ} - \tau\}$ and $\{\alpha^{0^\circ}|\beta^{90^\circ} - \tau - \alpha^{0^\circ}|\beta^{270^\circ} - \tau\}$ work as usual SSFP

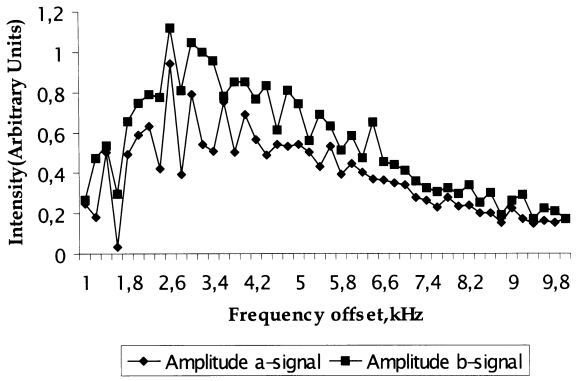

Fig. 7. The amplitude of a-signal and b-signal vs. frequency offset in the $\{\alpha^{0^\circ}|\beta^{90^\circ}-\tau-\alpha^{180^\circ}|\beta^{90^\circ}-\tau\}$ pulse sequence. Time spacing τ = 1.7 msec, $t_1 = t_2 = t_3 = t_4$ = 30 μs, 10 g of RDX inside solenoidal coil.

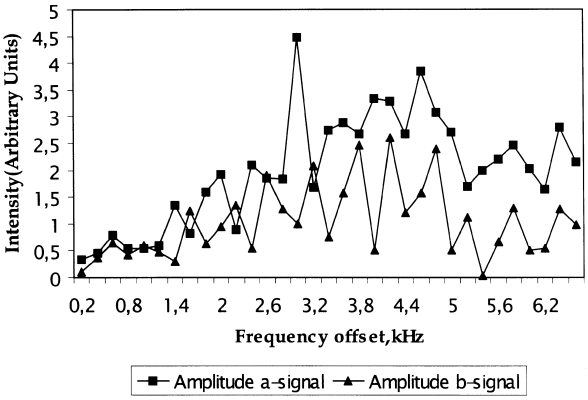

Fig. 8. The amplitude of a-signal and b-signal vs. frequency offset in the $\{\alpha^{0^\circ}|\beta^{90^\circ}-\tau-\alpha^{0^\circ}|\beta^{270^\circ}-\tau\}$ pulse sequence. Time spacing τ=1.8 msec, $t_1 = t_2 = t_3 = t_4$ = 35 μs, 10 g of RDX inside solenoidal coil.

sequence in the situation with not optimal pulse width. The presence of a- and b-signals in one observation window between two pairs of pulses is more visible for small τ. The frequency offset dependencies are shown in Figs 7 and 8. The shapes of the dependencies in Fig. 7 are similar to the dependencies of the amplitude of the FID and echo without the overlap of these signals. The curves for the other sequence, $\{\alpha^{0^\circ}|\beta^{90^\circ}-\tau-\alpha^{0^\circ}|\beta^{270^\circ}-\tau\}$, are shown in Figure 8. In this sequence the b-signal has a more complicated form which differs from that of the b-signal in the sequence $\{\alpha^{0^\circ}|\beta^{90^\circ}-\tau-\alpha^{180^\circ}|\beta^{90^\circ}-\tau\}$. From the analysis of (6 - 8) one derives that the b-signal consists of different components. The sum of these echo-components produces a complicated dependence of the amplitude on the frequency offset. It is necessary to make the more accurate calculation for a description of these signals.

The application of these composite sequences permits to improve the condition of remote NQR. In this case if we observe signals from the objects removed from the surface of the radio frequency coil, and if the dimensions of the objects are comparable with the dimensions of the coil, it is also difficult to achieve optimum pulse duration. This is connected with the great inhomogeneity of the radio frequency electromagnetic field at different points of the object. Therefore the use of a 90° phase shift in the composite pulse in a multi-pulse sequence SSFP or SORC offers the simplest improvement. The experimental investigation shows that not optimal pulse duration produces the a- and b-signal inside in observation window. However, the influence of these components is not dominant in a wide range.

Conclusion

The following conclusions can be derived from the analysis of the experimental data and theoretical results in this work:

1. The application of the multipulse sequences SSFP and SORC is problematic in remote detection of explosives. The overlaps of the FID and echo produce damping signals from the objects with different temperature properties. The increasing of time spacing τ for the division of FID and echo results in a reduction of the detection speed.

2. The application of the pulse sequences $\{\alpha^{0^\circ}|\beta^{90^\circ}-\tau-\alpha^{180^\circ}|\beta^{90^\circ}-\tau\}$ and $\{\alpha^{0^\circ}|\beta^{90^\circ}-\tau-\alpha^{0^\circ}|\beta^{270^\circ}-\tau\}$ permits to improve the condition of the detection without loss of effectiveness.

3. These sequences are more effective if the durations of the pulses are equal and the durations of pulses are close to 90°.

4. The actions of the sequences $\{\alpha^{0^\circ}|\beta^{90^\circ}-\tau-\alpha^{180^\circ}|\beta^{90^\circ}-\tau\}$ and $\{\alpha^{0^\circ}|\beta^{90^\circ}-\tau-\alpha^{0^\circ}|\beta^{270^\circ}-\tau\}$ can be explained by (6 - 8).

Acknowledgement

The author would like to express gratitude to Prof. V. P. Anferov from Kaliningrad State University and Patric Warren from Thorlock Corporation Ltd., Australia, for help in preparing the experiments.

[1] T. Hirshfeld and S. M. Klainer, J. Mol. Structure **58**, 63 (1980).
[2] J. P. Yesinovski, M. L. Buess, A. N. Garroway, M. Ziegeweid, and A. Pines. Anal. Chem. **67**), 2256 (1995).
[3] V. P. Anferov, G. V. Mozjoukhine, and R. Fisher, Rev. Sci. Instrum. **71**, 1656 (2000).
[4] A. J. Blauch, J. L. Schiano, and M. D. Ginsberg, J. Mag. Res. **139**, 139 (1999).
[5] H. Y. Carr, Phys. Rev. **112**, 1963 (1958).
[6] S. S. Kim, J. R. P. Jayakody, and R. A. Marino, Z. Naturforsch. **47a**, 415 (1992).
[7] S. M. Klainer, T. B. Hirschfeld, and R. A. Marino, Fourier transform nuclear quadrupole resonance spectroscopy, Fourier Hadamard and Hilbert Transform in Chemistry, Plenum, N. Y. 1982, p.147-181.
[8] D. Ya. Osokin, JETP, **115**, 1580 (1999).
[9] M. L. Buess, A. N. Garroway, and J. P. Yesinowsky, US Patent No 5,365,171 Nov. 15, 1994.
[10] V. P. Anferov and G. V. Mozjoukhine, Izvestia Vuzov, Fizika **9**, 47 (1999).
[11] G. V. Mozjoukhine, Applied Mag. Res. **18**, 527 (2000).
[12] K. L. Sauer, B. H. Suits, A. N. Garroway, and J. B. Miller, Chem. Phys. Lett. **342**, 362 (2001).
[13] B. C. Sanctuary, M. S. Krishnan, Z. Naturforsch. **49a**, 71 (1994).
[14] A. Ramamoorthy, and P. T. Narasimhan, J. Molecular Structure **192**, 333 (1989); S. Z. Ageev, D. J. Isbister, and B. C. Sanctuary, Molecular Physics, **83**, 193 (1994).
[15] G. V. Mozjoukhine, Appl. Mag.Res., in press (2001).
[16] A. J. Blauch, J. L. Schiano, and M. D. Ginsberg. J. Mag. Res. **139**, 139 (1999).